Published in final edited form as:
Phys Med Biol. 2012 December 7; 57(23): N493–N499. doi:10.1088/0031-9155/57/23/N493.

A simple Fourier transform-based reconstruction formula for photoacoustic computed tomography with a circular or spherical measurement geometry

Kun Wang and **Mark A. Anastasio**[§]
Department of Biomedical Engineering, Washington University in St. Louis, St. Louis, MO, 63130 USA

Abstract

Photoacoustic computed tomography (PACT), also known as optoacoustic tomography, is an emerging imaging modality that has great potential for a wide range of biomedical imaging applications. In this Note, we derive a hybrid reconstruction formula that is mathematically exact and operates on a data function that is expressed in the temporal frequency and spatial domains. This formula explicitly reveals new insights into how the spatial frequency components of the sought-after object function are determined by the temporal frequency components of the data function measured with a circular or spherical measurement geometry in two- and three-dimensional implementations of PACT, respectively. The structure of the reconstruction formula is surprisingly simple compared with existing Fourier-domain reconstruction formulae. It also yields a straightforward numerical implementation that is robust and two orders of magnitude more computationally efficient than filtered backprojection algorithms.

Photoacoustic computed tomography (PACT) is an emerging imaging modality that has great potential for a wide range of biomedical imaging applications (Oraevsky & Karabutov, 2003; Wang, 2008; Kruger, et al., 1999). In PACT, biological tissues of interest are illuminated by use of short laser pulses, which results in the generation of internal acoustic wavefields via the thermoacoustic effect (Xu & Wang, 2006; Xu, et al., 2010). The initial amplitudes of the induced acoustic wavefields are proportional to the spatially variant absorbed optical energy density within the tissues. The propagated acoustic wavefields are subsequently detected by use of a collection of ultrasonic transducers that are located outside the object. An image reconstruction algorithm is employed to estimate the absorbed optical energy density within the tissue from these data.

A variety of image reconstruction algorithms have been proposed for PACT (Xu, et al., 2002; Finch, et al., 2004; Xu & Wang, 2005; Finch, et al., 2007; Kunyansky, 2007; Hristova, et al., 2008; Kunyansky, 2012; Salehin & Abhayapala, 2012; Treeby & Cox, 2010). While iterative image reconstruction methods hold great value due to their ability to incorporate accurate models of the imaging physics and the instrument response (Paltauf, et al., 2002; Yuan & Jiang, 2007; Zhang, et al., 2009; Provost & Lesage, 2009; Wang, et al., 2011; Guo, et al., 2010; Huang, et al., 2010; Xu, et al., 2011; Buehler, et al., 2011; Bu, et al., 2012; Wang, et al., 2012), they can lead to long reconstruction times, even when accelerated by use of modern computing hardware such as graphics processing units (Wang et al., 2012). This is especially problematic in three-dimensional (3D) implementations of PACT, in which reconstruction times can be excessively long. Almost all experimental studies of PACT to date have employed analytic image reconstruction algorithms. Even if an iterative

[§]To whom correspondence should be addressed (anastasio@wustl.edu).

image reconstruction algorithm is to be employed, it is often useful to employ an analytic reconstruction algorithm to obtain a preliminary image that can initialize the iterative algorithm and thereby accelerate its convergence.

Most analytic reconstruction algorithms for PACT with a spherical measurement aperture and point-like transducers have been formulated in the form of filtered backprojection (FBP) algorithms. These algorithms possess a large computational burden, requiring $O(N^5)$ floating point operations to reconstruct a 3D image of dimension N^3. Image reconstruction algorithms based on the time-reversal principle and finite-difference schemes require $O(N^4)$ operations (Burgholzer, et al., 2007). Fast reconstruction algorithms for spherical measurement apertures that require only $O(N^3 \log N)$ operations have been proposed (Kunyansky, 2012; Salehin & Abhayapala, 2012). However, numerical implementations of these formulas require computation of special functions and multidimensional interpolation operations in Fourier space, which require special care to avoid degradation in reconstructed image accuracy. It is well-known that the temporal frequency components of the pressure data recorded on a spherical surface are related to the Fourier components of the sought-after object function (Anastasio, et al., 2007). However, to date, a simple reconstruction algorithm based on this relationship, i.e., one that does not require series expansions involving special functions or multi-dimensional interpolations, has yet to be developed.

In this Note, we derive a novel reconstruction formula for two-dimensional (2D) and 3D PACT employing circular and spherical measurement geometries, respectively. The mathematical forms of the reconstruction formulae are the same in both dimensions and are surprisingly simple compared with existing Fourier-domain reconstruction formulae for spherical and circular measurement geometries. The reconstruction formulae are mathematically exact and describe explicitly how the spatial frequency components of the sought-after object function are determined by the temporal frequency components of the measured pressure data. Their discrete implementations require only discrete Fourier transform, one-dimensional interpolation, and summation operations. A preliminary computer-simulation study is conducted to corroborate the validity of the reconstruction formula.

We consider the canonical PACT imaging model in which the object and surrounding medium are assumed to possess homogeneous and lossless acoustic properties and the object is illuminated by a laser pulse with negligible temporal width. Point-like, unfocused, ultrasonic transducers are assumed. We also assume that the effects of the acousto-electric impulse responses of the transducers have been deconvolved from the measured voltage signals so that the measured data can be interpreted as pressure signals. The 3D problem is addressed where $p(\mathbf{r}, t)$ denotes the photoacoustically-induced pressure wavefield at location $\mathbf{r} \in \mathbb{R}^3$ and time $t \geq 0$. However, the analysis and reconstruction formula that follows remains valid for the 2D case. The imaging physics is described by the photoacoustic wave equation (Oraevsky & Karabutov, 2003; Wang, 2008; Kruger et al., 1999):

$$\nabla^2 p(\mathbf{r}, t) - \frac{1}{c^2} \frac{\partial^2 p(\mathbf{r}, t)}{\partial^2 t} = 0, \quad (1)$$

subject to the initial conditions:

$$p(\mathbf{r}, t)\big|_{t=0} = \frac{\beta c^2}{C_p} A(\mathbf{r}); \quad \frac{\partial p(\mathbf{r}, t)}{\partial t}\Big|_{t=0} = 0, \quad (2)$$

where ∇^2 denotes the 3D Laplacian operator and $A(\mathbf{r})$ is the object function to be reconstructed that is contained within the volume V. Physically, $A(\mathbf{r})$ represents the

distribution of absorbed optical energy density. The constant quantities β, c, and C_p denote the thermal coefficient of volume expansion, speed-of-sound, and the specific heat capacity of the medium at constant pressure, respectively.

Let $p(\mathbf{r}_s, t)$ denote the pressure data recorded at location $\mathbf{r}_s \in S$ on a spherical surface S of radius R_S that encloses V. The continuous form of the imaging model that relates the measurement data to object function can be expressed as (Cox & Beard, 2005):

$$p(\mathbf{r}_s, t) = \mathscr{H} A \equiv \frac{\beta c^2}{C_p (2\pi)^3} \int_\infty d\mathbf{k}\, \widehat{A}(\mathbf{k}) \cos(ckt) e^{i\mathbf{k}\cdot\mathbf{r}_s}, \quad (3)$$

where $\mathbf{k} \in \mathbb{R}^3$ is the spatial frequency vector conjugate to $\mathbf{r}$, $k \equiv |\mathbf{k}|$, and $\hat{A}(\mathbf{k})$ is the 3D Fourier transform of $A(\mathbf{r})$. We adopt the Fourier transform convention

$$\widehat{A}(\mathbf{k}) = \mathscr{F}_3 A(\mathbf{r}) \equiv \int_\infty d\mathbf{r}\, A(\mathbf{r}) e^{-i\mathbf{k}\cdot\mathbf{r}} \quad (4a)$$

$$A(\mathbf{r}) = \mathscr{F}_3^{-1} \widehat{A}(\mathbf{k}) \equiv \frac{1}{(2\pi)^3} \int_\infty d\mathbf{k}\, \widehat{A}(\mathbf{k}) e^{i\mathbf{k}\cdot\mathbf{r}}. \quad (4b)$$

The imaging model in Eqn. (3) can be interpreted as a mapping $\mathscr{H}: O \rightarrow D$ between infinite dimensional vector spaces that contain the object and data functions. We will define O as the vector space of bounded and smooth functions that are compactly supported within the volume V.

Let the infinite set of functions $\{\gamma_\mu(\mathbf{r})\}$, indexed by μ, represent an orthonormal basis for O. The object function $A(\mathbf{r})$ can be represented as

$$A(\mathbf{r}) = \int_\infty d\mu \, \langle A, \gamma_\mu \rangle \gamma_\mu(\mathbf{r}), \quad (5)$$

where the inner product in O is defined as

$$\langle A, \gamma_\mu \rangle \equiv \int_V d\mathbf{r}\, A(\mathbf{r}) \gamma_\mu(\mathbf{r}) = \frac{1}{(2\pi)^3} \int_\infty d\mathbf{k}\, \widehat{A}(\mathbf{k}) \widehat{\gamma}_\mu(\mathbf{k}), \quad (6)$$

$\hat{\gamma}_\mu(\mathbf{k}) = \mathscr{F}_3 \gamma_\mu(\mathbf{r})$, and the quantity on the right-hand side of Eqn. (6) follows from fact that the Fourier transform is an isometry. A trace identity (see Eqn. (1.7) in reference (Finch et al., 2004) for the 3D case and Eqn. (1.16) in (Finch et al., 2007) for the 2D case) can be employed to relate the inner products in the spaces O and D as:

$$\langle A, \gamma_\mu \rangle = \frac{2C_p^2}{R_S \beta^2 c^2} \int_0^\infty dt \int_S d\mathbf{r}_s\, t\, p(\mathbf{r}_s, t) v_\mu(\mathbf{r}_s, t), \quad (7)$$

where

$$v_\mu(\mathbf{r}_s, t) = \mathscr{H} \gamma_\mu = \frac{\beta c^2}{C_p (2\pi)^3} \int_\infty d\mathbf{k}\, \widehat{\gamma}(\mathbf{k}) \cos(ckt) e^{i\mathbf{k}\cdot\mathbf{r}_s}, \quad (8)$$

and the right-hand side of Eqn. (7) defines a scaled version of the inner product in D.

On substitution from Eqn. (8) into Eqn. (7), one obtains

$$\langle A, \gamma_\mu \rangle = \frac{1}{(2\pi)^3} \int_\infty d\mathbf{k}\, \widehat{y}(\mathbf{k}) \widehat{\gamma}_\mu(\mathbf{k}), \quad (9)$$

where

$$\widehat{y}(\mathbf{k}) \equiv \frac{2C_p}{R_S \beta} \int_S d\mathbf{r}_s e^{i\mathbf{k}\cdot\mathbf{r}_s} \int_0^\infty dt\, tp(\mathbf{r}_s, t) \cos(ckt). \quad (10)$$

Comparison of Eqns. (6) and (9) reveals that $\hat{A}(\mathbf{k}) = \hat{y}(\mathbf{k})$. By evaluating the Fourier cosine transform that is present in the right-hand side of Eqn. (10), a reconstruction formula for determining $\hat{A}(\mathbf{k})$ can therefore be expressed as

$$\widehat{A}(\mathbf{k}) = \frac{2C_p}{R_S \beta} \int_S d\mathbf{r}_s e^{i\mathbf{k}\cdot\mathbf{r}_s} \mathrm{Re}\left\{ \mathscr{F}_1 \left\{ tp(\mathbf{r}_s, t) \right\} (\mathbf{r}_s, \omega)|_{\omega = ck} \right\}, \quad (11)$$

where $\mathscr{F}_1$ denotes the one-dimensional (1D) Fourier transform with respect to time t and 'Re' denotes the operation that takes the real part of quantity in the brackets. Subsequently, $A(\mathbf{r})$ is determined as $\mathscr{F}_3^{-1} \widehat{A}(\mathbf{k})$.

Equation (11) represents a novel reconstruction for PACT and is the key result of this Note. Unlike previously proposed Fourier-domain reconstruction formulae (Norton, 1980; Kunyansky, 2012; Salehin & Abhayapala, 2012), Eqn. (11) has a simple form and does not involve series expansions utilizing special functions. The reconstruction formula reveals that the measured data $p(\mathbf{r}_S, t)$ determine the 3D Fourier components of the $A(\mathbf{r})$ via a simple process that involves the following four steps: (1) Compute the 1D temporal Fourier transform of the modified data function $tp(\mathbf{r}_S, t)$; (2) Isolate the real-valued component of this quantity corresponding to temporal frequency $\omega = ck$; (3) Weight this value by the plane-wave $e^{i\mathbf{k}\cdot\mathbf{r}_S}$; and (4) Sum the contributions, formed in this way, corresponding to every measurement location $\mathbf{r}_S \in S$. This reveals the components of $\hat{A}(\mathbf{k})$ residing on a sphere of radius $\frac{k}{c}$ are determined by the 1D Fourier transform of $tp(\mathbf{r}_S, t)$ corresponding to temporal frequency ω. In this sense, Eqn. (11) can be interpreted as an implementation of the Fourier Shell Identity (Anastasio et al., 2007). Finally, the form of Eqn. (11) remains unchanged in the 2D case, where $\mathbf{r}_S, \mathbf{k} \in \mathbb{R}^2$ and S is a circle that encloses the object.

A discrete implementation of Eqn. (11) possesses low computational complexity and desirable numerical properties. The 1D fast Fourier transform (FFT) can be employed to approximate the action of $\mathscr{F}_1$ and only a 1D interpolation is required to determine the value of the Fourier transformed data function corresponding to temporal frequency $\omega = ck$, where k corresponds to the magnitude of vectors $\mathbf{k}$ that specify a 3D Cartesian grid. From the values of $\hat{A}(\mathbf{k})$ determined on this grid, the 3D FFT algorithm can be employed to estimate values of $A(\mathbf{r})$. If the object is represented on a $N \times N \times N$ grid and the number of transducer locations and time samples are both $\mathcal{O}(N)$, the computational complexity is limited by the 3D FFT algorithm, i.e., $\mathcal{O}(N^2 \log N)$ in 2D and $\mathcal{O}(N^3 \log N)$ in 3D.

A preliminary computer-simulation study for the 2D case was conducted to corroborate the correctness of the reconstruction formula. The object function $A(\mathbf{r})$ was taken to be the numerical phantom shown in Fig. 1-(a), which was comprised of a collection of uniform disks that were blurred by a 2D Gaussian kernel whose full-width-at-half-maximum was 0.3

mm. The phantom was discretized by use of pixel expansion functions with a pitch of 0.025 mm. The measurement geometry consisted of 256 point-like transducers that were uniformly distributed over a circle of radius 12.8 mm that enclosed the object. The k-wave toolbox (Treeby & Cox, 2010) was employed to numerically solve the photoacoustic wave equation and generate simulated pressure signals at each transducer location at a temporal sampling rate of 30 MHz. The simulated pressure data set generated in this way contained 256 × 2048 data samples. The speed-of-sound and $\frac{\beta}{C_p}$ were assigned values of 1.5-mm/μs and 1000 (arbitrary units), respectively. A noisy data set was produced by addition of 5% uncorrelated Gaussian noise to the noiseless pressure data.

Images were reconstructed on a uniform 2D grid of spacing 0.1 mm by use of a discretized form of Eqn. (11) coupled with the 2D inverse FFT algorithm. In order to reconstruct images of dimension 256 × 256, samples of $\hat{A}(\mathbf{k})$ were determined on a uniform 2D grid of dimension 512 × 512 with a sampling interval of $(0.1 \times 256)^{-1}$ mm^{-1}. The samples of the data function $tp(\mathbf{r}_s, t)$ were zero-padded by a factor of 8 prior to estimating its 1D Fourier transform by use of the FFT algorithm. From these data, nearest neighbor 1D interpolation was employed to determine the values of the term in brackets in Eqn. (11) corresponding to $\omega = ck$ for the sampled locations $\mathbf{k}$.

The images reconstructed from the noiseless and noisy data sets are shown in Fig. 1-(b) and (c). Profiles corresponding to the central rows of these images are shown in Fig. 2. These results confirm that the proposed reconstruction algorithm can reconstruct images with high fidelity from noise-free measurement data. Although, a systematic investigation of the noise propagation properties of the proposed algorithm is beyond the scope of this Note, Figs. 1-(c) and 2-(b) suggest that its performance is robust in the presence of noise. This is to be expected, since all operations involved in the implementation of Eqn. (11) are numerically stable.

In summary, we have derived a Fourier-based reconstruction formula for PACT employing circular and spherical measurement apertures. The formula is mathematically exact and possesses a surprisingly simple form compared with existing Fourier-domain reconstruction formulae. The formula yields a straightforward numerical implementation that is stable and is two orders of magnitude more computationally efficient than 3D filtered backprojection algorithms. The proposed formula serves as an alternative to existing fast Fourier-based reconstruction formulae. A systematic comparison of the proposed reconstruction formula with existing formulae by use of experimental data remains an important topic for future studies.

Acknowledgments

This work was supported in part by NIH awards EB010049 and CA167446.

References

Anastasio MA, et al. Application of inverse source concepts to photoacoustic tomography. Inverse Problems. 2007; 23:S21–S35.

Bu S, et al. Model-Based Reconstruction Integrated With Fluence Compensation for Photoacoustic Tomography. Biomedical Engineering, IEEE Transactions on. 2012; 59(5):1354–1363.

Buehler A, et al. Model-based optoacoustic inversions with incomplete projection data. Medical Physics. 2011; 38(3):1694–1704. http://link.aip.org/link/?MPH/38/1694/1. [PubMed: 21520882]

Burgholzer P, et al. Exact and approximative imaging methods for photoacoustic tomography using an arbitrary detection surface. Phys Rev E. 2007; 75:046706.

Cox BT, Beard PC. Fast calculation of pulsed photoacoustic fields in fluids using k-space methods. The Journal of the Acoustical Society of America. 2005; 117(6):3616–3627. [PubMed: 16018465]

Finch D, et al. Inversion of Spherical Means and the Wave Equation in Even Dimensions. SIAM Journal on Applied Mathematics. 2007; 68(2):392–412.

Finch D, et al. Determining a function from its mean values over a family of spheres. SIAM Journal of Mathematical Analysis. 2004; 35:1213–1240.

Guo Z, et al. Compressed sensing in photoacoustic tomography in vivo. Journal of Biomedical Optics. 2010; 15(2):021311. http://link.aip.org/link/?JBO/15/021311/1. [PubMed: 20459233]

Hristova Y, et al. Reconstruction and time reversal in thermoacoustic tomography in acoustically homogeneous and inhomogeneous media. Inverse Problems. 2008; 24(5):055006.

Huang, C., et al. Investigation of limited-view image reconstruction in optoacoustic tomography employing a priori structural information. Vol. 7800. SPIE; 2010. p. 780004http://link.aip.org/link/?PSI/7800/780004/1

Kruger R, et al. Thermoacoustic computed tomography-technical considerations. Medical Physics. 1999; 26:1832–1837. [PubMed: 10505871]

Kunyansky LA. Explicit inversion formulae for the spherical mean Radon transform. Inverse Problems. 2007; 23:373–383.

Kunyansky LA. Fast reconstruction algorithms for the thermoacoustic tomography in certain domains with cylindrical or spherical symmetries. Inverse Problems and Imaging. 2012; 6(1):111–131.

Oraevsky, AA.; Karabutov, AA. Optoacoustic Tomography. In: Vo-Dinh, T., editor. Biomedical Photonics Handbook. CRC Press LLC; 2003.

Norton S. Reconstruction of a two-dimensional reflecting medium over a circular domain: Exact solution. Journal of the Acoustical Society of America. 1980; 67(4):1266–1273.

Paltauf G, et al. Iterative reconstruction algorithm for optoacoustic imaging. The Journal of the Acoustical Society of America. 2002; 112(4):1536–1544. http://link.aip.org/link/?JAS/112/1536/1. [PubMed: 12398460]

Provost J, Lesage F. The Application of Compressed Sensing for Photo-Acoustic Tomography. Medical Imaging, IEEE Transactions on. 2009; 28(4):585–594.

Salehin SMA, Abhayapala TD. Frequency-radial duality based photoacoustic image reconstruction. The Journal of the Acoustical Society of America. 2012; 132(1):150–161. [PubMed: 22779464]

Treeby BE, Cox BT. k-Wave: MATLAB toolbox for the simulation and reconstruction of photoacoustic wave fields. Journal of Biomedical Optics. 2010; 15(2):021314. [PubMed: 20459236]

Wang K, et al. An Imaging Model Incorporating Ultrasonic Transducer Properties for Three-Dimensional Optoacoustic Tomography. Medical Imaging, IEEE Transactions on. 2011; 30(2): 203–214.

Wang K, et al. Investigation of iterative image reconstruction in three-dimensional optoacoustic tomography. Physics in Medicine and Biology. 2012; 57(17):5399. [PubMed: 22864062]

Wang LV. Tutorial on Photoacoustic Microscopy and Computed Tomography. IEEE Journal of Selected Topics in Quantum Electronics. 2008; 14:171–179.

Xu M, Wang LV. Photoacoustic imaging in biomedicine. Review of Scientific Instruments. 2006; 77(041101)

Xu Y, et al. Exact frequency-domain reconstruction for thermoacoustic tomography: I. Planar geometry. IEEE Transactions on Medical Imaging. 2002; 21:823–828. [PubMed: 12374319]

Xu Y, Wang LV. Universal back-projection algorithm for photoacoustic computed tomography. Physical Review E. 2005; 71(016706)

Xu Z, et al. Photoacoustic tomography of water in phantoms and tissue. Journal of Biomedical Optics. 2010; 15(3):036019. http://link.aip.org/link/?JBO/15/036019/1. [PubMed: 20615021]

Xu Z, et al. In vivo photoacoustic tomography of mouse cerebral edema induced by cold injury. Journal of Biomedical Optics. 2011; 16(6):066020. [PubMed: 21721821]

Yuan Z, Jiang H. Three-dimensional finite-element-based photoacoustic tomography: Reconstruction algorithm and simulations. Medical Physics. 2007; 34(2):538–546. http://link.aip.org/link/?MPH/34/538/1. [PubMed: 17388171]

Zhang J, et al. Effects of Different Imaging Models on Least-Squares Image Reconstruction Accuracy in Photoacoustic Tomography. Medical Imaging, IEEE Transactions on. 2009; 28(11):1781–1790.

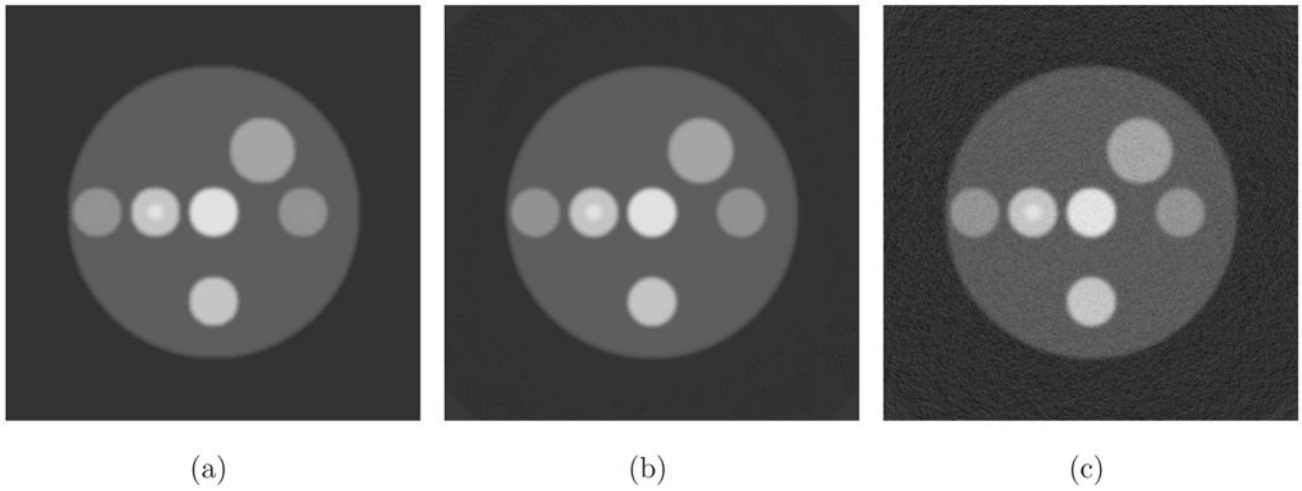

Figure 1.
The numerical phantom is shown in subfigure (a). Images reconstructed by use of the proposed reconstruction algorithm from noiseless and noisy data are shown in subfigures (b) and (c), respectively. The greyscale window is [−0.2, 1.2].

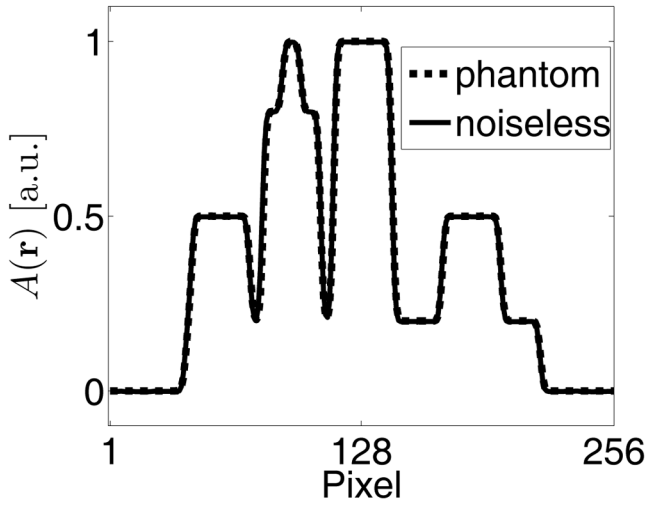

(a)

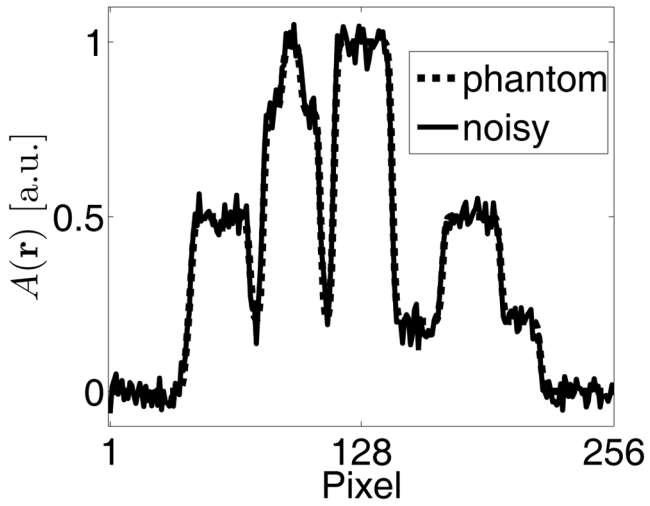

(b)

Figure 2.
Profiles corresponding to the central rows of the images shown in Fig. 1-(b) (subfigure(a)) and Fig. 1-(c) (subfigure(b)). The solid line in subfigure (a), which corresponds to the image reconstructed from noiseless data, almost completely overlaps with the profile through the numerical phantom.